J A C S
JOURNAL OF THE AMERICAN CHEMICAL SOCIETY

A New Class of Ionically Conducting Fluorinated Ether Electrolytes with High Electrochemical Stability

Chibueze V. Amanchukwu, Zhiao Yu, Xian Kong, Jian Qin, Yi Cui,* and Zhenan Bao*

Cite This: https://dx.doi.org/10.1021/jacs.9b11056

ABSTRACT: Increasing battery energy density is greatly desired for applications such as portable electronics and transportation. However, many next-generation batteries are limited by electrolyte selection because high ionic conductivity and poor electrochemical stability are typically observed in most electrolytes. For example, ether-based electrolytes have high ionic conductivity but are oxidatively unstable above 4 V, which prevents the use of high-voltage cathodes that promise higher energy densities. In contrast, hydrofluoroethers (HFEs) have high oxidative stability but do not dissolve lithium salt. In this work, we synthesize a new class of fluorinated ether electrolytes that combine the oxidative stability of HFEs with the ionic conductivity of ethers in a single compound. We show that conductivities of up to 2.7×10^{-4} S/cm (at 30 °C) can be obtained with oxidative stability up to 5.6 V. The compounds also show higher lithium transference numbers compared to typical ethers. Furthermore, we use nuclear magnetic resonance (NMR) and molecular dynamics (MD) to study their ionic transport behavior and ion solvation environment, respectively. Finally, we demonstrate that this new class of electrolytes can be used with a Ni-rich layered cathode (NMC 811) to obtain over 100 cycles at a C/5 rate. The design of new molecules with high ionic conductivity and high electrochemical stability is a novel approach for the rational design of next-generation batteries.

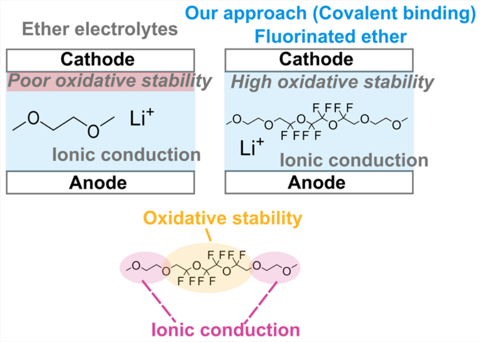

■ INTRODUCTION

The availability of energy-dense and compact batteries has galvanized interest in the electrification of transport and further integration of renewables in the grid. Rechargeable lithium-ion batteries are the batteries of choice today because they have the highest energy densities (~250 W h/kg).[1,2] However, their energy densities and cost are currently insufficient to keep pace with our insatiable demand for longer range electric vehicles and a reduction in our carbon footprint.[1] Li-ion batteries use graphite as the anode, a mixture of carbonates as the electrolyte, and a transition metal oxide (TMO) such as $LiCoO_2$ as the cathode. To obtain higher energy densities, battery chemistries such as lithium−high-voltage TMO (~440 W h/kg), lithium−sulfur (~650 W h/kg), and lithium−air (~950 W h/kg) have been heavily explored.[1−4] These improvements in energy density are predicated on the use of lithium metal as the anode because of its high theoretical specific capacity (3860 mA h/g_{Li}) and low reduction potential (−3.04 V).[2,5−7] However, lithium metal reacts significantly with the electrolyte (because of the low reduction potential) to generate a solid electrolyte interface (SEI).[8] Unlike in graphite where the SEI can be quite robust and sustains long-term cycling, the SEI on lithium metal is quite porous, and continuous electrolyte degradation leads to cell death.[9] Electrolyte stability against the cathode is also of great interest because of the existence of electrodes such as Ni-rich $LiNi_{0.8}Mn_{0.1}Co_{0.1}O_2$ (NMC 811) with capacities much higher than NMC 111 used commercially today. However, accessing the energy density in Ni-rich NMC 811 requires high charging cutoff potentials (at least 4.4 V or above).[10] Increasing the oxidative stability of electrolytes while maintaining stable lithium metal deposition/stripping and high ionic conductivities is a great challenge, because the electrochemical stability window shifts between different classes of electrolytes.[11]

There are two classes of electrolytes that dominate the lithium metal literature: carbonates and ethers. Carbonates such as ethylene carbonate (EC) and ethyl methyl carbonate (EMC) are currently used in today's lithium-ion batteries because of their high dielectric constant (and high ionic conductivities), and the ability of EC to form a robust SEI on graphite.[9] Unfortunately, when carbonates are used in lithium metal batteries, the SEI is porous, and side reactions with lithium metal are exacerbated, leading to low Coulombic efficiencies.[9,12] Therefore, typical carbonates used in lithium-ion batteries have been eschewed for ethers in lithium metal batteries. Ethers such as 1,3-dioxolane (DOL) and 1,2-

Received: October 14, 2019
Published: April 1, 2020

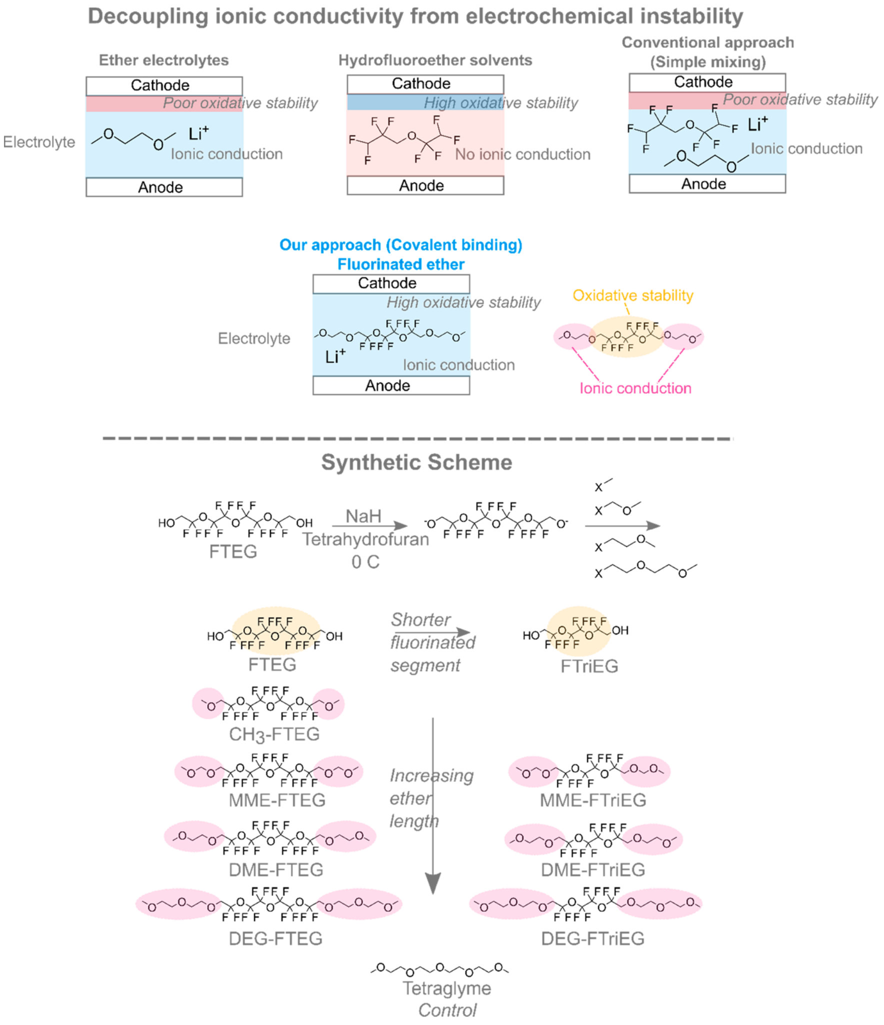

Figure 1. Motivation and synthetic scheme. Illustration of typical challenges with common electrolytes. Ethers support ion conduction but have poor oxidative stability. Hydrofluoroethers have high oxidative stability but support no ion conduction. Simply mixing hydrofluoroethers and ethers at typical 0.1 or 1 M salt concentrations still suffers from poor oxidative stability. Covalently attaching an ether to the hydrofluoroether allows for both high ionic conductivity and oxidative stability (our approach). Synthesis of fluorinated ethers through deprotonation of fluorinated tetraethylene glycol (FTEG) and fluorinated triethylene glycol (FTriEG) and subsequent addition of varying alkoxy halides. The fluorinated segment is varied between FTEG and FTriEG to understand the effect of the fluorinated group, and the ether group is varied from MME to DME to DEG to understand the effect of ether type and length. Tetraglyme (shown) serves as the control for comparisons.

dimethoxyethane (DME) also support high ionic conductivities, and high Coulombic efficiencies for lithium metal deposition and stripping.[13,14] However, ethers at typical 0.1 or 1 M salt concentrations cannot be used with Ni-rich NMC 811 or other high-voltage cathodes because of the low oxidative stability of ethers (less than 4 V vs Li/Li^+).[14−16] Therefore, there is great need for the design and synthesis of new electrolytes to support both lithium metal and high-voltage cathodes.

Several electrolyte engineering strategies are typically pursued to improve oxidative stability. For example, solvent-in-salt systems—with a high salt concentration in the electrolyte to decrease the “free” solvent concentration and mobility—have been shown to improve oxidative stability.[14,15,17,18] Unfortunately, the solvent-in-salt electrolytes have high viscosity, high cost, lower ionic conductivities, and slower reaction kinetics.[19−21] Another engineering approach involves additives such as hydrofluoroethers.[19] Hydrofluoroethers such as 1,1,2,2-tetrafluoroethyl-2,2,3,3-tetrafluoropropylether (TTE) and bis(2,2,2-trifluoroethyl) ether (BTFE) have found great use in lithium metal batteries as diluents for solvent-in-salt electrolytes.[22,23] These hydrofluoroethers do not dissolve any salt and have no ionic conductivity but have high oxidative stabilities (Figure 1).[24,25] Unfortunately, mixing these hydrofluoroethers (HFEs) with typical ethers does not significantly increase the oxidative stability of the overall electrolyte mixture. Therefore, a new approach (beyond electrolyte engineering) is highly desired to combine the high ionic conductivity of ether solvents with the high oxidative stability of hydrofluoroethers. Thus, we pursued an electrolyte chemistry approach.

Some ionically conductive fluorinated electrolytes have been synthesized by Balsara and DeSimone et al.,[26−30] but all of these systems have carbonate groups attached, which are undesired for lithium metal batteries as mentioned above. In this work, we show a novel method to combine high ionic conductivity with high oxidative stability in a single molecule by synthesizing a new class of fluorinated ether electrolytes (Figure 1). We vary the length and type of ether group, and the length of the fluorinated segment to obtain structure−property

https://dx.doi.org/10.1021/jacs.9b11056

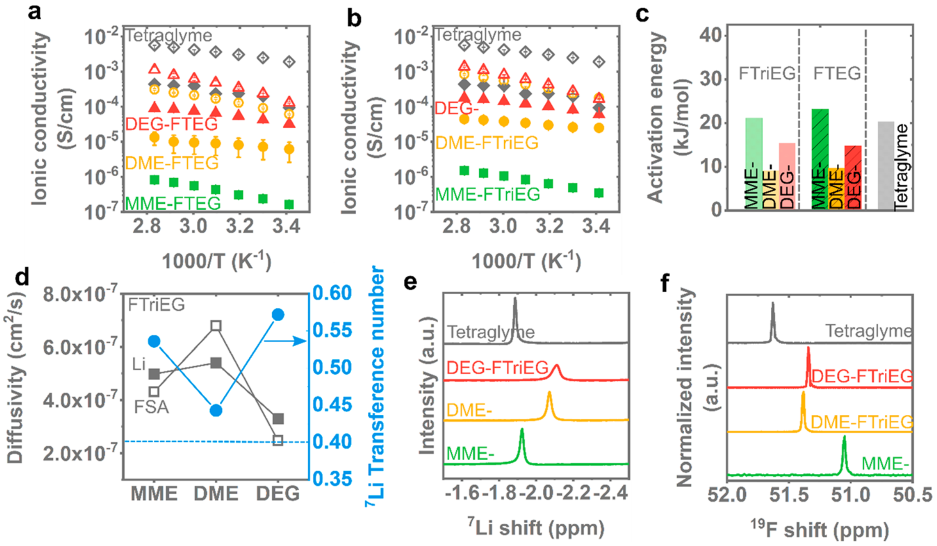

Figure 2. Ionic transport and conductivity. Ionic conductivity as a function of LiFSA salt content (closed symbol −0.1 M, open symbol −1 M) for (a) FTEG compounds and (b) FTriEG compounds with tetraglyme as the control in both. All the data points in the conductivity plots have error bars representing the standard deviation from at least three different cells. (c) Activation energy obtained from Arrhenius fits of conductivity versus temperature for 0.1 M LiFSA salt concentration. (d) Lithium (^{7}Li) cation and FSA (^{19}F) anion diffusivities and lithium (^{7}Li) transference number obtained through pulsed field gradient NMR for 0.1 M LiFSA in FTriEG compounds. The dashed line at 0.4 represents the lithium transference number in tetraglyme. Measured diffusivity for Li (1.28×10^{-6} cm^2/s) and FSA (1.93×10^{-6} cm^2/s) in 0.1 M LiFSA tetraglyme. Corresponding (e) lithium (^{7}Li) and (f) fluorine (^{19}F) shifts for the lithium cation and the FSA anion for 0.1 M LiFSA dissolved in FTriEG compounds and tetraglyme.

relationships. We show that the molecules (although liquid at room temperature with low molecular weight) actually have glass transitions instead of melting transitions of typical ethers. Ionic conductivity within this class of compounds is higher with longer ether groups and with a shorter fluorinated segment, and we show conductivities as high as 2.7×10^{-4} S/cm (at 30 °C) and lithium transference numbers higher than typical ethers (tetraglyme). In addition to the high ionic conductivity, these compounds also have high oxidative stabilities up to 5.6 V (at least 1.4 V greater than tetraglyme or a tetraglyme:TTE mixture), showing the powerful combination of covalently attaching an ether segment for high ionic conductivity and a fluorinated segment for high oxidative stability in a single molecule. Using nuclear magnetic resonance (NMR) spectroscopy and molecular dynamics (MD) simulations, we study the influence of electrolyte structure on ionic transport, diffusivity, and salt solvation structure. Finally, we show that this class of electrolytes is promising for high-voltage Li-NMC 811 batteries supporting over 100 cycles at rates as high as C/5. Our approach to obtain high ionic conductivity and electrochemical stability in the same compound can be explored with other solvent classes such as nitriles and sulfones and increase the number of electrolytes of interest for battery chemistries. Designing new electrolytes with novel properties is essential to revolutionize our energy landscape and bring batteries closer to fulfilling their great promise.

■ RESULTS AND DISCUSSION

Rationale for Molecular Design. The rationale for molecular design was guided by the need to combine the oxidative stability of hydrofluoroethers such as BTFE/TTE with the ionic conductivity properties of ethers (Figure 1). Ether solvents have high ionic conductivities but suffer from poor oxidative stability.[15,18] In contrast, hydrofluoroethers have high oxidative stability but cannot dissolve lithium salts.[19,24,25] Conventionally, the literature has pursued a mixing approach,[31] but as we will show, a simple mixture does not combine the benefits of both classes of compounds because the mixture is still limited by one of the components with low oxidative stability. In this work, we pursue a covalent approach where a fluorinated core is covalently bound to the ether "end group". Hence, the fluorinated core can lead to high oxidative stability and support Ni-rich cathodes such as $LiNi_{0.8}Mn_{0.1}Co_{0.1}O_2$ (NMC 811) with a high charge cutoff, while the ether group imbues the compound with high salt dissolution and ionic conductivity (Figure 1). In this manner, the design accomplishes an ionically conductive fluorinated ether. We avoid carbonate functionality because of their poor stability against lithium metal.[9,12] We chose tetraglyme as our control because it has been heavily studied,[15,32,33] and the ether length is comparable to our synthesized fluorinated ethers. Meanwhile, our ability to vary the length of both the fluorinated and ether segments in a modular fashion allows for systematic study of structure−property relationships.

Synthesis and Confirmation of Structure. Fluorinated ethers were synthesized by functionalizing fluorinated glycols with alkoxy halides (Figure 1). Commercially available fluorinated tetraethylene glycol (FTEG) and fluorinated triethylene glycol (FTriEG) were deprotonated using sodium hydride. After deprotonation, varying alkoxy halides were added to substitute the terminal group. The modular nature of this synthesis allows for a library of possible compounds. By moving from FTEG to FTriEG, we can understand the effect of the fluorinated length on ionic conductivity, oxidative stability, and subsequent properties. The ether length can be tuned from methyl methyl ether (MME) to dimethyl ether (DME) to understand the effect of the spacer group (methylene vs ethylene) while maintaining the total number of oxygen groups. A comparison of DME to diethylene glycol

(DEG) makes it possible to understand the effect of ether length. We use alkoxy halides for ease of synthesis because halides are facile leaving groups, although their cost can be a hindrance. For DEG-FTEG, we synthesize using tosyl leaving groups showing the versatility of our approach (see the Experimental Section). Once functionalized, flash column chromatography was used to purify the compounds, and nuclear magnetic resonance (NMR) spectroscopy (Figure S1) and Fourier transform infrared (FTIR) spectroscopy (Figure S2) were used to confirm the structure and product purity.

Thermal Properties. The thermal properties of the compounds were characterized. Figure S3 shows decomposition and/or evaporation profiles obtained using thermogravimetric analysis (TGA), where the lengths of the ether and fluorinated segments dictate the temperature at which evaporation occurs. Differential scanning calorimetry (DSC) was used to study the thermal behavior of the fluorinated ethers. Figure S4 shows cooling traces at a rate of 5 °C/min after a prior heating run. The starting glycol reactants (FTEG and FTriEG) have crystallization peaks (after the heating cycle created a melt), and tetraglyme also has a crystallization peak.[16] However, the fluorinated ethers do not have melting transitions, but glass transitions (T_g) around −21 °C. Despite the low scan rates used, the molecules are unable to pack to form a crystal, a behavior that has also been observed for other bulky small molecules.[34] Finally, the T_g seems insensitive to changes in either fluorinated or ether segments.

Ionic Conductivity and Transport Mechanism. The ionic conductivity of lithium salts dissolved in the fluorinated compounds was examined using electrochemical impedance spectroscopy (EIS). Figure 2a,b shows conductivity as a function of temperature for different salt concentration and fluorinated ether combinations. We chose lithium bis(fluorosulfonyl)amide (LiFSA) salt for this work because it can dissolve in concentrations larger than 1 M in all the synthesized compounds (except for CH_3-FTEG which was not studied further). Figure 2a shows that as the spacer group increases from ($-CH_2O-$) in MME-FTEG to ($-CH_2CH_2O-$) in DME-FTEG, there is a 30× increase in ionic conductivity at 30 °C (Table S1). Furthermore, as one increases the ether length from DME-FTEG to DEG-FTEG, there is only a 6× increase. The FTriEG compounds in Figure 2b also corroborate the effect of ether length on ionic conductivity as observed with the FTEG compounds in Figure 2a. Furthermore, an increase in salt concentration from 0.1 to 1 M also leads to an increase in ionic conductivity as expected. Finally, as the fluorinated segment is shortened from FTEG to FTriEG, there is also an increase in ionic conductivity (Figure 2b). The 1 M LiFSA in DEG-FTriEG electrolyte has the highest ionic conductivity at 2.7×10^{-4} S/cm at 30 °C; conductivities in the range of 10^{-4} S/cm and above are relevant for electrochemical systems. However, the conductivity of 1 M LiFSA in tetraglyme is still an order of magnitude higher at 30 °C.

The conductivity dependence on temperature can be fitted using an Arrhenius form (Figure S5) to obtain the activation energy barrier for ion transport. The insignificant shift in T_g precluded the use of the Vogel−Tammann−Fulcher (VTF) form. Although Figure 2a,b showed a direct correlation between ether length and conductivity, the correlation with activation energy is nuanced (Figure 2c and Figure S5). The activation energy is a function of only ether spacer type and ether length. For 0.1 M electrolytes, DME-FTriEG electrolyte has lower activation energies compared to MME-FTriEG, DEG-FTriEG, and tetraglyme. The difference in activation energy barrier is surprising because DEG-FTriEG and tetraglyme support higher ionic conductivities than DME-FTriEG. The FTEG compounds behave similarly (Figure 2c), and increasing the salt concentration does not change the activation energy trends between both the FTriEG and FTEG compounds (Figure S5).

The different trends in activation energy barrier prompted further spectroscopic study of the ionic transport environment within the electrolytes. We use pulsed field gradient (PFG) NMR to probe lithium (^{7}Li for Li^+) and anion (^{19}F for FSA^-) diffusion. Figure 2d shows diffusivity within the FTriEG class of compounds. Remarkably, the trend for Li^+ and FSA^- diffusivity mirrors the activation energy trend in Figure 2c. Li^+ and FSA^- diffusivity is highest in DME-FTriEG than in MME or DEG-FTriEG. Despite the lower ionic conductivity in MME-FTriEG compared to DEG-FTriEG, lithium diffuses faster, an observation we partly attribute to the lower viscosity of MME compared to DEG-FTriEG (Table S2). Furthermore, within DME-FTriEG, FSA^- diffuses faster than Li^+ whereas Li^+ diffuses faster than FSA^- in MME and DEG-FTriEG. Using PFG NMR, Figure 2d shows that the lithium transference number ($t_{Li^+} = \frac{D_{Li^+}}{D_{Li^+} + D_{FSA^-}}$) is higher in MME and DEG-FTriEG compared to DME-FTriEG. A similar trend in transference numbers is also observed for the FTEG class of compounds (Figure S6). Despite these differences, these compounds have higher lithium transference numbers compared to tetraglyme ($t_{Li+} = 0.4$). Figure S7 shows mean squared displacement (MSD) for 1 M LiFSA dissolved in MME-FTriEG, DME-FTriEG, and tetraglyme, and the lithium transference number trends match our experimental results; however, simulations tend to underestimate diffusion coefficients.[35,36] Balsara et al.[26−30] have shown that carbonate-terminated perfluoropolyether compounds also show a higher transference number compared to a carbonate solvent control. Furthermore, these compounds show higher transference numbers compared to previously reported LiTFSI in perfluoropolyether (PFPE):polyethylene glycol (PEG) blends.[31]

The ion binding environment was also examined using ^{7}Li and ^{19}F NMR. An NMR capillary setup was used for ^{7}Li NMR (see the Experimental Section) and the data referenced to a 1 M $LiClO_4$ in acetonitrile internal standard (−2.80 ppm).[37] Within the FTriEG family, as one moves from MME to DME to DEG, an upfield shift is observed (Figure 2e), which could be due to stronger ion solvation or an increase in ion-pairing; unfortunately Figure 2e alone is insufficient to distinguish between the two as both phenomena will lead to upfield shifts.[38−40] Figure 2f shows the ^{19}F chemical shift where a downfield trend is observed for FSA^- as one increases the ether length. Compared to tetraglyme, the peaks are upfield, signaling increased Li^+ ion-pairing with the FSA anion or also stronger binding between the FSA anion and the fluorinated ether.[38] Between Figure 2e and 2f, the shifts from MME to DME are much greater ($\Delta = 0.15$ ppm ^{7}Li and 0.34 ppm ^{19}F) than moving from DME to DEG ($\Delta = 0.04$ ppm ^{7}Li and 0.05 ppm ^{19}F), indicating that the spacer group effect especially relating to ionic solvation ($-CH_2O-$ to $-CH_2CH_2O-$) is more dominant than the ether length effect ($-CH_2CH_2O-$ to $-CH_2CH_2OCH_2CH_2O-$). Figure S8 shows that similar chemical shift trends are observed within the FTEG class of compounds, although DEG-FTEG has more of a downfield

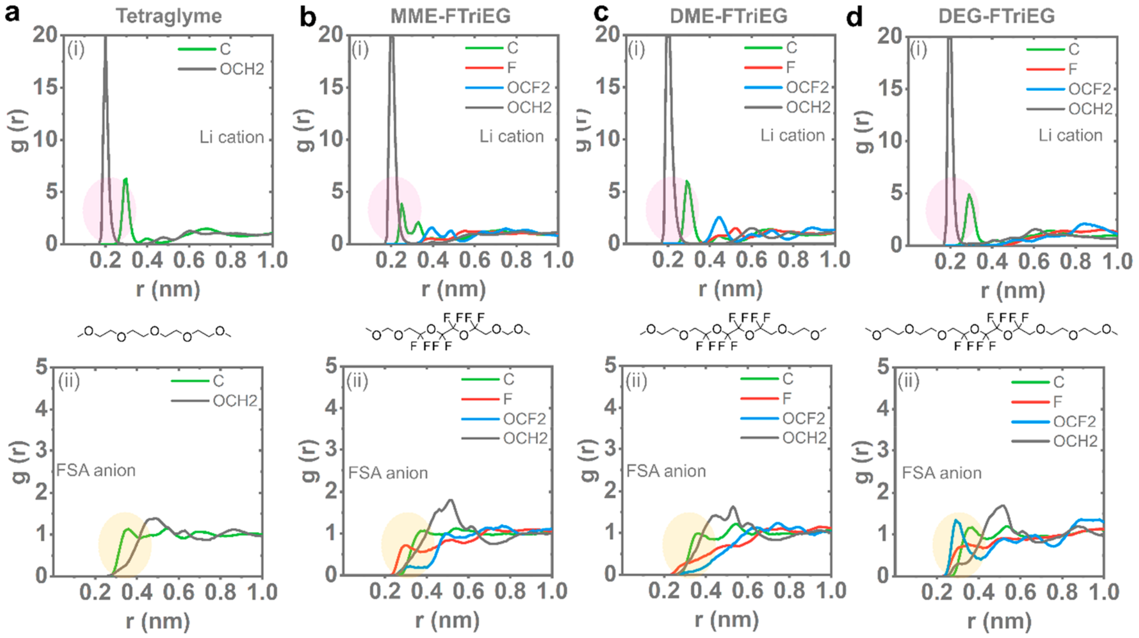

Figure 3. Salt solvation structure in the electrolyte. Radial distribution functions (RDFs) of 0.1 M LiFSA in the different electrolytes: (a) tetraglyme, (b) MME-FTriEG, (c) DME-FTriEG, and (d) DEG-FTriEG. The highlighted regions are to draw attention to the differences between the spectra for both the lithium cation and the FSA anion. The chemical structures are added for ease of comparison. $-OCF_2$ and $-OCH_2$ in the legends allow for differentiation of which oxygen atom is adjacent to either the cation or anion, where $-OCF_2$ represents the oxygen from the fluorinated component, and $-OCH_2$ represents the oxygen from the ether end groups. (i) Lithium cation and (ii) FSA anion for the respective electrolytes. The anion spectra in part ii refer to the interaction between the fluorine atom in the FSA anion and the respective compounds.

shift compared to DEG-FTriEG. ^{7}Li spin−lattice relaxation times (T_1), where relaxation occurs by translational and rotational motion, were measured as a function of temperature for FTriEG and FTEG compounds (Figure S9).[22,41] As a quadrupolar nuclei, ^{7}Li can also undergo quadrupolar relaxation mechanisms.[22] Figure S9 shows that tetraglyme has the longest T_1, and the T_1 decreases as one goes from MME to DEG (in both FTriEG and FTEG), with the DEG compounds having the shortest T_1. Unfortunately, the T_1 values correlate with viscosity of the fluorinated ethers, which does not allow for easy delineation on the impact of ion pair formation on T_1 relaxation.

Ionic Solvation Structure. Molecular dynamics (MD) simulations were performed to better understand the lithium and anion solvation environment within these fluorinated ethers (Figure 3 and Figure S10). Figure 3 shows radial distribution functions (RDFs) for the lithium cation and the FSA anion in tetraglyme and the FTriEG compounds at a 0.1 M concentration. As Figure 3a shows, the oxygen (with its lone pair) on the ether group (OCH_2) of tetraglyme has the highest probability of being adjacent to the lithium cation. Figure S10 shows the RDF for CH_3-FTEG, and both OCH_2 and OCF_2 are adjacent to the lithium cation. The high OCF_2 peak coincides with the first peak of OCH_2, implying that OCH_2 and OCF_2 have comparable interaction with Li^+. Since OCF_2 does not support lithium transport, this means that CH_3-FTEG has poor solvation power for Li^+, which may explain the observed low solubility of LiFSA in CH_3-FTEG (<0.1 M LiFSA solubility). Comparing the RDFs for lithium in Figure 3b−d shows the ether group adjacent to the lithium cation. This supports the hypothesis shown in Figure 1 where the ether segment in the fluorinated ether coordinates with lithium and supports its transport. Comparing Figure 3bi,ci shows that as one moves from the methylene to the ethylene spacer unit, there is less interference from the carbon within the first solvation shell, and an increased probability of the carbon being in the next solvation shell. Also, looking at Figure 3bi,ci,di shows that as the ether length is increased, the probability of OCF_2 in the lithium solvation shell diminishes. Again, this may help explain why increasing the ether length leads to higher ionic conductivities.

The increase in transference number observed here was also observed by Balsara et al.[26,29] and attributed to the interaction between the fluorinated ether and the anion. We remarked about the nonlinear trend involving MME-, DME-, and DEG-FTriEG regarding the activation energy and lithium transference numbers in Figure 2c,d. Figure S11 shows RDF analyses at a 1 M LiFSA concentration in the fluorinated ether electrolytes, and they show that both F and H atoms from the solvent contribute significantly to the interaction with the FSA anion. Therefore, it appears that the fluorinated segment in these compounds interacts significantly with the fluorinated anion through the “fluorous effect” hence inhibiting anionic transport (which is desired): a hypothesis originally proposed by Balsara et al.,[29] but no conclusive evidence was provided until this work. However, for DME-FTriEG, Figure S11 shows that the binding between the ether group (labelled as the O−H peak) is much higher than in MME-FTriEG and DEG-FTriEG, slowing lithium ion diffusion and explaining the lower lithium transference number observed experimentally. Figure 2d corroborates the MD data by showing that FSA^- diffuses faster than Li^+ in DME-FTriEG (as also observed with tetraglyme). Therefore, the ether segment in the fluorinated ether coordinates with lithium while the fluorinated segment coordinates preferentially with the FSA anion. All these fluorinated ethers have higher transference numbers compared to tetraglyme because the fluorine group in the fluorinated ether interacts with the anion, albeit to different degrees.

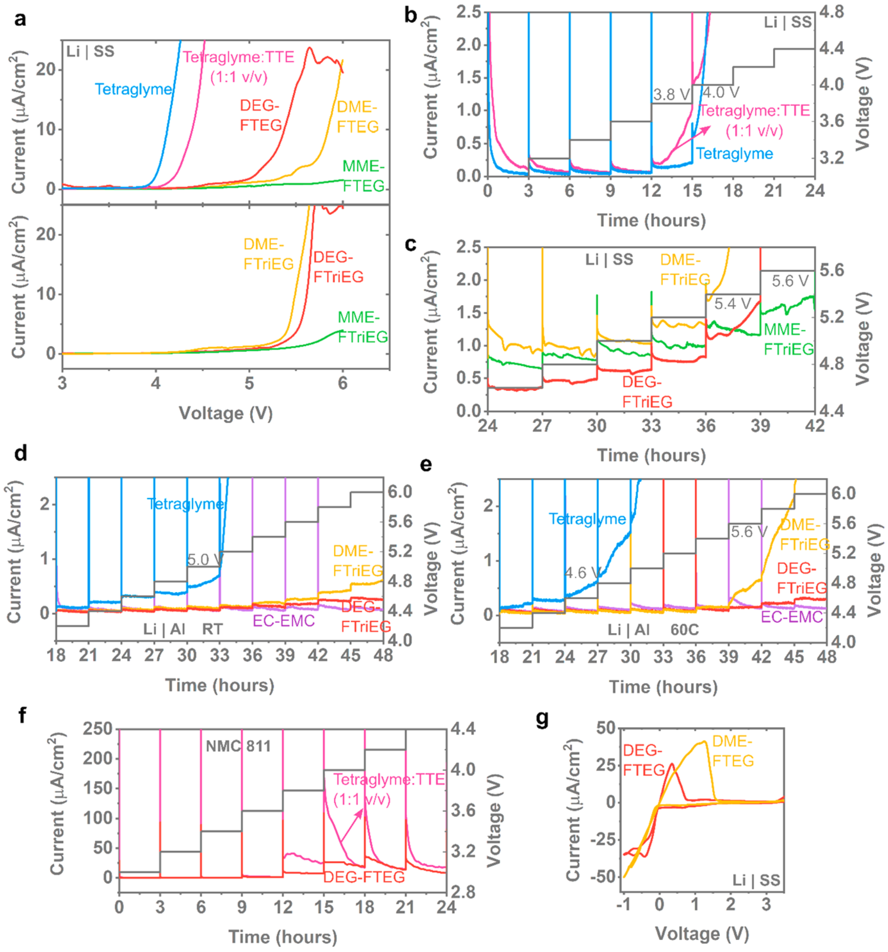

Figure 4. Oxidative and reductive stability. (a) Linear sweep voltammetry at 0.1 mV/s with FTEG compounds, FTriEG compounds, tetraglyme, and a tetraglyme:TTE (1:1 v/v) mixture with a stainless steel (SS) working electrode and 0.1 M LiFSA salt concentration. Potentiostatic holds for 3 h at different voltages with stainless steel as the working electrode and 0.1 M LiFSA in (b) tetraglyme and tetraglyme:TTE (1:1 v/v) and (c) FTriEG electrolytes. Potentiostatic holds with aluminum (Al) foil as the working electrode and 1 M LiFSA salt concentration in tetraglyme, DME-FTriEG, DEG-FTriEG, and 1 M $LiPF_6$ in EC-EMC (3:7 v/v) at (d) room temperature (RT) and (e) 60 °C. Potentiostatic holds with (f) NMC 811 as the working electrode in 0.1 M LiFSA in DEG-FTEG and the tetraglyme:TTE (1:1 v/v) mixture. (g) Cyclic voltammetry scanning reductively at 0.1 mV/s with 0.1 M LiFSA in FTEG compounds and a stainless steel working electrode. Reference and counter electrode: lithium metal. EC-EMC = ethylene carbonate:ethyl methyl carbonate. RT = room temperature.

Oxidative and Reductive Stability. The oxidative stability of these fluorinated ethers was explored. Our motivation for synthesizing this new class of electrolytes is to couple high ionic conductivity with high oxidative stability in a single molecule. Figure 4a shows a linear sweep voltammetry (LSV) plot with a scan rate of 0.1 mV/s from open circuit to 6 V. As the data remarkably shows, all the fluorinated ethers have oxidative voltages at least 1.4 V greater than tetraglyme (Table S1). Furthermore, the oxidative voltage is a function of ether length with MME-FTriEG and MME-FTEG showing excellent stability. We also studied the oxidative stability of a simple yet typically studied mixture of tetraglyme:TTE in a 1:1 volume ratio (1:1.45 molar ratio), and Figure 4a shows that the oxidative stability of the mixture is still poor compared to the synthesized fluorinated ethers, further validating our design strategy in Figure 1 that focuses on covalently attaching ethers to the fluorinated segment instead of simple mixing. The result is intriguing because, despite the presence of ethers in the synthesized fluorinated compounds, there is still a significant improvement in oxidative stability. For example, DEG-FTriEG has more ether groups than tetraglyme, but the oxidative voltage is still higher (>5.1 V vs 4 V). In addition, the oxidative stability in Li/SS cells is not influenced by increasing the salt concentration from 0.1 to 1 M (Figures S12 and S13). The inductive electron-withdrawing effect of fluorine shifts electron density away from the oxygen groups within the ether segment, decreasing the ether propensity for oxidation.[9,42,43] Another evidence of the shift in electron density is the lowered ability of the ether segment in the FTEG and FTriEG compounds to coordinate and transport lithium (Figure 2). We believe the accessibility of the ether group to the electrode surface is also limited in the fluorinated ether compared to tetraglyme, where the fluorinated segment may orient toward the electrode surface limiting ether accessibility to the surface. Somorjai et al.[44] have previously shown using sum frequency generation (SFG) vibrational spectroscopy that when a fluorinated compound is adjacent to an electrode (e.g., amorphous silicon), it reorients to expose the CF_3 groups to the surface to form an ordered fluorine-dominated passivation layer on the electrode surface. Although our synthesized compounds do not have fluorinated terminal groups, our observation of high oxidative stability despite the presence of ethers lends credence to the importance of electrolyte orientation on oxidative stability. Our strategy could provide great utility in the design of new electrolytes with greater electrochemical stability.

We also use potentiostatic holds to further probe the oxidative stability of the fluorinated compounds.[45] Using a stainless steel, aluminum, or Ni-rich NMC 811 electrode with different electrolytes, we hold the potential for 3 h at increasingly higher potentials and record the current response. If no undesired Faradaic reactions are occurring, the current should decay.[45] Potentiostatic hold experiments for long times are less susceptible to the influence of impurities that could lead to early current rise—earlier than the true compound oxidation—in LSV experiments. Therefore, we quote the oxidative voltages from potentiostatic hold experiments. Figure 4b shows current response as a function of voltage comparing tetraglyme and the simple tetraglyme:TTE (1:1 v/v) mixture with a stainless steel electrode. The tetraglyme or tetraglyme:TTE mixture shows an oxidative stability between 3.8 and 4 V, as previously reported.[46] Meanwhile, Figure 4c shows a similar setup but with the FTriEG compounds, and the oxidative stabilities increase up to 5.4−5.6 V. Significant increases in oxidative stability are also observed with the FTEG compounds (Figure S14 and Table S1). However, continuous stainless steel corrosion at earlier voltages is observed at 60 °C for both FTriEG compounds and tetraglyme (Figure S13). Although stainless steel electrodes provide great information on oxidative stability, they are not practically relevant. We also explored the oxidative stability of 1 M salt concentration in fluorinated ethers in commercially relevant Li/Al cells at room temperature and at 60 °C (Figure 4d,e). Aluminum is currently used as the current collector in commercial lithium-ion cells, but imide salts such as LiFSA have been eschewed in commercial cells because of Al corrosion.[8,21,43,47] Figure 4d,e shows that these fluorinated ethers can passivate the Al surface and are stable at high voltages: similar to commercial 1 M $LiPF_6$ in EC:EMC (ethylene carbonate:ethyl methyl carbonate) (3:7 v/v) electrolytes and much better again than 1 M LiFSA in tetraglyme. Typically, very high LiFSA salt concentrations are required when Al is used, but these fluorinated ether electrolytes allow for normal 1 M salt concentration.[21] Since, we are interested in stability against high-voltage cathode systems, we also performed potentiostatic holds with NMC 811 as the electrode. Figure 4f shows a comparison between the tetraglyme:TTE mixture and DEG-FTEG. The uninhibited current rise observed in Figure 4b,c is not seen with NMC 811, but the tetraglyme:TTE mixture shows higher currents at around 3.8−4 V as observed in Figure 4b. Meanwhile, the DEG-FTEG electrolyte shows much improved stability.

The ability to support lithium metal deposition and stripping was also investigated. Supporting efficient cycling of lithium metal is vital, and Figure 4g and Figure S15 show that the electrolytes can support lithium metal deposition and stripping. Figure S16 shows lithium/lithium cells cycled in various electrolytes where DEG-FTriEG can support long-term Li/Li cycling (comparably to tetraglyme and 1 M $LiPF_6$ in EC-EMC commercial electrolytes) albeit with higher overpotentials due to the lower ionic conductivity of the fluorinated electrolytes. In addition, Figure S17 shows Li/Cu cells where a 1 M LiFSA in DEG-FTriEG electrolyte supports more efficient lithium cycling similar to 1 M LiFSA in tetraglyme, but much better than a commercial 1 M $LiPF_6$ in EC:EMC electrolyte.

Investigation with a High-Voltage Cathode. The ability of these novel electrolytes to support battery cycling was investigated. Electrolytes with high oxidative stability are desired for next-generation cathode materials with higher energy densities such as NMC 811. To probe the influence of our electrolyte, we use an NMC 811 electrode (theoretical capacity ~203 mA h/g)[10] with a loading of 4 mg/cm^2 and cycled from 3 to 4.4 V. Figure 5a shows a cell with 1 M LiFSA in tetraglyme as the electrolyte with NMC 811 as the cathode cycled at a current rate of C/10. By the first charge, the cathode cannot be charged to the cutoff as undesired side reactions occur.[48] Although the cell can be discharged to low capacity (~50 mA h/g), the second charge is quite poor as the electrolyte is continuously consumed.[48] In contrast, Figure 5b shows significant improvement in cycling when 1 M LiFSA in DEG-FTriEG is used as the electrolyte even with a 4.4 V charge cutoff. We chose DEG-FTriEG for exploration in a battery because it has the highest ionic conductivity of the compounds explored in this work, and high oxidative stability. The cycling result is exciting because it shows that the significant increase in oxidative stability has enabled cycling of a Ni-rich cathode. Figure 5c shows long-term cycling at C/10 and C/5 current rates for over 100 cycles. The Coulombic efficiency observed in the Li/Cu cell in Figure S17 is lower than that in Figure 5c and may be due to the larger surface area lithium that is deposited in a Li/Cu cell that will continuously react with the electrolyte. The ability to couple high ionic conductivity and high oxidative stability has enabled the operation of an ionically conductive fluorinated ether as the electrolyte in a high-voltage lithium−metal-based battery.

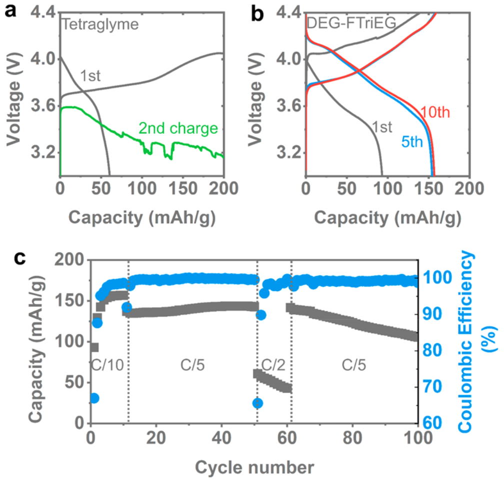

Figure 5. Battery performance. Galvanostatic cycling of 1 M LiFSA in (a) tetraglyme and (b) DEG-FTriEG with an NMC 811 cathode (~0.9 mA h/cm^2) at a current rate of C/10. (c) Discharge capacity and Coulombic efficiency as a function of cycle number for the 1 M LiFSA in DEG-FTriEG electrolyte.

■ CONCLUSIONS

New electrolytes are vital for high-energy-density battery chemistries. However, currently used ether electrolytes have low oxidative stability (<4 V), whereas typical hydrofluoroethers currently used as diluents have high oxidative stability but cannot dissolve lithium salts. In this work, we show a novel method to combine the high ionic conductivity of ethers with the high oxidative stability of fluorinated compounds into a single molecule. We synthesize a variety of new fluorinated ether compounds and obtain structure−property relationships. These compounds have ionic conductivities as high as 2.7×10^{-4} S/cm at 30 °C, and oxidative voltages as high as 5.6 V (4 V in tetraglyme). Remarkably, LiFSA imide salt does not corrode aluminum in the presence of these fluorinated ethers at a typical 1 M concentration, and the fluorinated electrolytes have oxidative stability characteristics similar to commercial carbonate electrolytes while enabling efficient lithium metal cycling. Importantly, we show that a simple mixture of tetraglyme with a widely used hydrofluoroether still suffers from low oxidative stability. Therefore, our approach of covalently combining the ether and the fluorinated segment allows for high ionic conductivity and high oxidative stability. Using NMR and MD simulations, we explore structure−property relationships and show that ionic conductivity in our fluorinated ether increases with longer ether segment and shorter fluorinated segment. We show that the high transference number is due to specific interactions between the anion and the fluorinated segment. Finally, we fabricate batteries using NMC 811 as the cathode with a loading of 4 mg/cm^2 and show that the cells can be cycled over 100 times using these fluorinated ethers, and current rates up to C/5 are accessible. The combination of all these properties in a class of new electrolytes is exciting and will inspire the design and synthesis of new electrolyte structures for next-generation battery systems.

■ EXPERIMENTAL SECTION

Materials. Fluorinated tetraethylene glycol (FTEG) (98% purity), fluorinated triethylene glycol (FTriEG) (98% purity), 1,1,2,2-tetrafluoroethyl-2,2,3,3-tetrafluoropropylether (TTE) (98%+ purity), and lithium bis(fluorosulfonyl)amide (99% purity) were obtained from Oakwood Chemical and Synquest Laboratories. 1-Bromo-2-(2-methoxyethoxy) ethane (>90% purity) and sodium hydride (60% in paraffin oil) were obtained from TCI America. 2-Bromoethyl methyl ether (>85% purity), iodomethyl methyl ether (90% purity, with copper stabilizer), and tetraglyme (>99%) were obtained from Sigma-Aldrich. Lithium metal (750 μm thickness) was obtained from Alfa Aesar. Deuterated acetonitrile (D, 99.8%) was obtained from Cambridge Isotope Laboratories. Aluminum foil was obtained from MTI. NMR capillary tubes were obtained from New Era Enterprises. LiPF$_6$ (1 M) in EC-EMC (3:7 v/v) (LP57) was obtained from Gotion.

Synthesis and Purification. *Synthesis of DEG-FTEG. Synthesis of 1-Tosyl-2-(2-methoxyethoxy) Ethane.* To a round-bottom flask were added 50 mL of dry THF (from solvent extraction system), 50 mL of 6 M NaOH solution, and 18 g of diethylene glycol methyl ether. The suspension was cooled to 0 °C with an ice bath, purged with nitrogen, and stirred for about 30 min. Tosyl chloride (∼54 g) was separately dissolved in 80 mL of dry THF and added dropwise using a syringe to the stirring suspension. The flask was stirred at 500 rpm and room temperature for 5 h. Thin layer chromatography (TLC) with UV detector was used to monitor the progress of the reaction.

After allowing the reaction to return to room temperature, the suspension was extracted by 300 mL of diethyl ether. The organic layer was washed with distilled water and dried with Na_2SO_4. The diethyl ether was removed under vacuo to yield a light yellow oil. The crude product was purified by flash column chromatography (methanol:dichloromethane = 10:90) to yield the final product as colorless oil for the next step.

Synthesis of DEG-FTEG. To a round-bottom flask were added ∼150 mL of dry THF (from solvent extraction system) and 2.5 mol equiv (relative to FTEG amount) of NaH. The suspension was cooled to 0 °C with an ice bath, purged with nitrogen, and stirred for about 20 min. FTEG (∼10 g) was separately dissolved in 20 mL of dry THF and added dropwise using a syringe to the suspension. Bubbling can be observed upon FTEG addition. The suspension was further stirred under nitrogen atmosphere at 0 °C for about 2 h. Then, 2.2 mol equiv (relative to FTEG amount) of 1-tosyl-2-(2-methoxyethoxy) ethane was added to the flask. More THF is added for a total of roughly 200 mL. The flask was stirred at 500 rpm and 100 °C under reflux for 5 h. Thin layer chromatography (TLC) with iodine staining was used to monitor the progress of the reaction.

After allowing the reaction to return to room temperature, the excess NaH was quenched by dropwise addition of isopropanol. The mixture was then rotavaped to remove most of the solvent. The residue was dissolved in a small amount of water and was neutralized by dumping into dilute HCl. The aqueous solution was then extracted with dichloromethane (∼200 mL × 3 times). The organic layer was washed with distilled water (or dilute HCl) and dried with Na_2SO_4. The dichloromethane was removed under vacuo to yield an orange oil. The crude product was purified by flash column chromatography [Teledyne-Isco] (ethyl acetate:hexanes = 15:85) to yield the final product as colorless oil. The product was then filtered off through a 0.45 μm PTFE filter and moved to an argon glovebox where it was then stored over 4 Å molecular sieves. NMR confirmation of structure can be found in Figure S1. Yield after purification: 30%.

Synthesis of DME-FTriEG. To a round-bottom flask were added ∼150 mL of dry THF (from solvent extraction system) and 5 mol equiv (relative to 10 g of FTriEG) of NaH (6.8 g of NaH). The suspension was cooled to 0 °C with an ice bath, purged with nitrogen, and stirred for about 20 min. FTriEG (∼10 g) was separately dissolved in 20 mL of dry THF and added dropwise using a syringe to the suspension. Bubbling can be observed upon FTriEG addition. The suspension was further stirred under nitrogen atmosphere at 0 °C for about 2 h. Then, 2.5 mol equiv (relative to FTriEG amount) of 2-bromoethyl methyl ether was added to the flask. More THF was added for a total of roughly 200 mL. The flask was stirred at 500 rpm and 80 °C under reflux for 2 days. Thin layer chromatography (TLC) with iodine staining was used to monitor the progress of the reaction.

After allowing the reaction to return to room temperature, the excess NaH was quenched by dropwise addition of isopropanol. The mixture was then rotavaped to remove most of the solvent. The residue was dissolved in a small amount of water and was neutralized by dumping into dilute HCl (0.1 M, 200 mL). The aqueous solution was then extracted with dichloromethane (∼200 mL × 3 times). The organic layer was washed with distilled water (or dilute HCl) and dried with Na_2SO_4. The dichloromethane was removed under vacuo to yield an orange oil. The crude product was purified by flash column chromatography (ethyl acetate:hexanes = 15:85) to yield the final product as colorless oil. The product was then filtered off through a 0.25 μm PTFE filter and moved to an argon glovebox where it was then stored over 4 Å molecular sieves. NMR was used to confirm product structure and purity (see the Supporting Information). NMR confirmation of structure can be found in Figure S1. Yield after purification: 48%.

Synthesis of DME-FTEG. Fluorinated tetraethylene glycol (10 g), 2-bromoethyl methyl ether (2.5 mol equiv), and sodium hydride (5 equiv) were used. Mole equivalents are relative to the FTEG starting amount. A similar procedure as detailed for DME-FTriEG was used. NMR confirmation of structure can be found in Figure S1. Yield after purification: 63%.

Synthesis of DEG-FTriEG. Fluorinated triethylene glycol (10 g), 1-bromo-2-(2-methoxyethoxy) ethane (2.5 mol equiv, 15.6 g), and sodium hydride (5 equiv, 6.8 g) were used. Mole equivalents are relative to the FTriEG starting amount.

A similar procedure as detailed for DME-FTriEG was used with the following additions: The reaction was refluxed at 80 °C for 3 nights. The sample was run through the flash column (50 wt % ethyl acetate, 50 wt % hexanes) four times to completely purify the product. The concentrated product was then filtered using a 0.45 μm PTFE filter and moved to an argon glovebox where it was stored under 4 Å molecular sieves. NMR confirmation of structure can be found in Figure S1. Yield after purification: 50%.

Synthesis of MME-FTriEG. A similar procedure as detailed for DME-FTriEG was used with the following additions: 2.2 mol equiv of iodomethyl methyl ether (10 g) was used for the reaction with 5 equiv of NaH (5.49 g) and 7.67 g of fluorinated triethylene glycol. Mole equivalents are relative to FTriEG starting amount. For flash column chromatography, a solvent mixture of hexane (95%) and ethyl acetate (5%) was used. NMR confirmation of structure can be found in Figure S1. Yield after purification: 78%.

Synthesis of MME-FTEG. A similar procedure as detailed for DME-FTriEG was used with the following additions: 2.2 mol equiv of iodomethyl methyl ether (10 g) was used for the reaction with 5 mol equiv of NaH (5.29 g) and 10.84 g of fluorinated tetraethylene glycol. Mole equivalents are relative to FTEG starting amount. For flash column chromatography, a solvent mixture of hexane (95%) and ethyl acetate (5%) was used. NMR confirmation of structure can be found in Figure S1. Yield after purification: 70%.

Synthesis of CH_3-FTEG. In a round-bottom flask, sodium hydride (5 g) was added to and stirred in dry tetrahydrofuran (~150 mL) and cooled to 0 °C. In a vial, FTEG (10 g) was first dissolved in THF (~20 mL) and was then added into the suspension dropwise. The flask was purged with nitrogen multiple times. The reaction was allowed to run for 2 h at 0 °C. Afterward, methyl iodide (2.5 equiv) was added dropwise, and the reaction was allowed to return to room temperature; it was stirred overnight. For flash column chromatography, a solvent mixture of hexane (90%) and ethyl acetate (10%) was used. NMR confirmation of structure can be found in Figure S1. Yield after purification: 75%.

Characterization. Fourier transform infrared (FTIR) spectroscopy was performed using a Nicolet iS50 FTIR spectrometer, and measurements were performed using ATR mode. Thermal gravimetric analysis (TGA) was performed using a TA Instrument Q500. DSC was performed using a TA Instrument Q2000. The samples for DSC were first cooled to −90 °C to reset any thermal history. Then, the samples were heated at 5 °C/min to 80 °C and then cooled at the same rate to −90 °C (this heating and cooling cycle is reported in the manuscript). Viscosity measurements were done using a TA ARES G2 rheometer with an 8 mm diameter stainless steel parallel plate geometry.

Nuclear Magnetic Resonance (NMR) Spectroscopy. NMR was used to confirm the synthesis of product and efficacy of purification. Once synthesized, purified, and filtered, a little amount of the compound was dissolved in deuterated DMSO, and NMR was performed. A Varian Inova 400 MHz instrument was used.

For NMR experiments for the electrolytes, an NMR capillary setup was used. Sample preparation was done inside an argon glovebox where 0.1 M LiFSA was dissolved in the different fluorinated compounds. The fluorinated compounds had been stored in 4 Å molecular sieves. The electrolytes were freshly prepared for the measurements. The electrolyte mixture was placed inside a capillary tube, sealed with a PTFE cap, and added to the NMR tube containing 1 M $LiClO_4$ in deuterated acetonitrile as the internal standard. We chose 1 M $LiClO_4$ in CD_3CN as the internal standard because both its ^{7}Li and ^{1}H shifts do not interfere with the compounds of interest. ^{7}Li, ^{1}H, and ^{19}F were performed using a Varian Inova 300 MHz and a Varian 400 MHz instrument.

Pulsed field gradient (PFG) NMR was used to study the diffusivity of lithium and anion in the respective fluorinated solvents. For the diffusivity measurements, the capillary setup was used, except that the 1 M $LiClO_4$ in CD_3CN internal standard was removed. The capillaries were placed in an empty 5 mm NMR tube. All diffusion measurements were made with the Varian 400 MHz instrument at a temperature of 20.7 °C (the temperature was not controlled to limit convection effects).[49] A convection compensation pulse sequence (program "Dbppste_cc") was used for the ^{7}Li diffusion (for lithium ion) measurements while no convection compensation was needed for the ^{19}F measurements (for the FSA anion) (program "pgste"). Gradient strengths of up to 15 G/cm were used, pulses of (^{19}F, $\delta = 0.005{-}0.01$ s and $\Delta = 0.15$ s; ^{7}Li, $\delta = 0.0075{-}0.01$ s and $\Delta = 0.15{-}0.6$ s). The peak intensity was used for the fitting, and diffusion constants were obtained by fitting the linearized version of the following equation:

$$I/I_0 = \exp\left(-\gamma^2 g^2 \delta^2 D\left(\Delta - \frac{\delta}{3}\right)\right)$$

where I = intensity as a function of gradient, γ = gyromagnetic ratio, g = gradient strength, δ = duration pulse, D = diffusion constant, and Δ = gradient pulse interval.

The lithium transference number was calculated using the diffusivity values obtained from PFG NMR and the following equation:

$$t_{\mathrm{Li}^+} = \frac{D_{\mathrm{Li}^+}}{D_{\mathrm{Li}^+} + D_{\mathrm{FSA}^-}}$$

Spin−lattice relaxation (T_1) measurements were made on a Varian Inova 300 MHz instrument. Temperature calibration was first done using a sealed ethylene glycol sample. The sample was allowed to equilibrate for 5 min at the desired temperature before the T_1 was measured. Measurements were done in heating mode.

Electrochemical Characterization. Ionic conductivity measurements were performed using coin cells (CR2032) with stainless steel (SS)/stainless steel (SS) blocking electrodes. Coin cells were fabricated in an argon glovebox in the following manner: SS‖20 μL‖1 Celgard 2325‖20 μL‖SS. SS (16.2 mm diameter), Celgard 2325 (25 μm thickness, 2 cm^2). Temperature sweeps (cooling mode) were done using an ESPEC environmental chamber. The cells were first held at 80 °C and then cooled to obtain 70, 60, 50, 40, 30, and 20 °C. The cells were held at each temperature for at least 2 h before cell impedance was measured. The cell constant is 7.75. The cell constant was obtained by fabricating coin cells with 1 M LiFSA in tetraglyme electrolyte and a PTFE spacer with a 1 cm^2 hole (2 cm^2 disk, 0.348 mm thickness). Comparing this result to the cell measured with Celgard separator allowed for a determination of the cell constant. A Biologic VSP3 instrument was used for the impedance measurements.

Battery Fabrication. Coin cells (CR2035) were used for battery fabrication. Li metal‖15 μL‖1 Celgard 2325‖15 μL‖electrode. For the oxidative and reductive stability experiments, the electrode was either stainless steel (16.2 mm diameter) or NMC 811 (12.7 mm). Cells were allowed to rest for 3−5 h before measurements were performed. A Biologic MPG2 or VSP3 potentiostat was used for all the measurements. For the 30 °C cells, an ESPEC environmental chamber was used to maintain constant temperature. (The NMC 811 electrode: 4 mg/cm^2, 8:1:1 mass ratio of NMC 811:PVdF:Super P carbon; PVdF = polyvinylidene fluoride).

Molecular Dynamics Simulation. The interactions between molecules/ions were described by the Optimized Potentials for Liquid Simulations all atom (OPLS-AA) based force field.[50] Atomic charges of the fluorinated ether solvents were calculated using Møller−Plesset second-order perturbation method with the correlation-consistent polarized valence cc-pVTZ(-f) basis set.[51] The simulation boxes contain one pair of LiFSA solvated in a particular number of solvents so that the salt concentration is approximately 0.1 M. The radial distribution functions were calculated from MD trajectories of 20 ns long. Larger simulation boxes with more than one pair of LiFSA were also tested and found no significant changes in the radial distribution functions. All MD simulations were conducted with the Gromacs 2018 program.[52] The temperature was controlled at 300 K using the Nosé−Hoover thermostat with a relaxation time of 0.2 ps while the pressure was controlled at 1 bar using the Parrinello−Rahman barostat with a relaxation time of 2.0 ps.

■ ASSOCIATED CONTENT

Supporting Information

The Supporting Information is available free of charge at https://pubs.acs.org/doi/10.1021/jacs.9b11056.

Additional data and figures including ^{1}H NMR, FTIR spectra, TGA data, DSC data, activation energy values, Li and FSA diffusivity, Arrhenius fits, RDFs, potentiostatic holds, LSV results, and CV data (PDF)

AUTHOR INFORMATION

Corresponding Authors

Yi Cui − *Department of Materials Science and Engineering, Stanford University, Stanford, California 94305, United States; Stanford Institute for Materials and Energy Sciences, SLAC National Accelerator Laboratory, Menlo Park, California 94025, United States;* orcid.org/0000-0002-6103-6352; Email: yicui@stanford.edu

Zhenan Bao − *Department of Chemical Engineering, Stanford University, Stanford, California 94305, United States;* orcid.org/0000-0002-0972-1715; Email: zbao@stanford.edu

Authors

Chibueze V. Amanchukwu − *Department of Chemical Engineering, Stanford University, Stanford, California 94305, United States;* orcid.org/0000-0002-6573-1213

Zhiao Yu − *Department of Chemistry, Stanford University, Stanford, California 94305, United States;* orcid.org/0000-0001-8746-1640

Xian Kong − *Department of Chemical Engineering, Stanford University, Stanford, California 94305, United States;* orcid.org/0000-0001-5602-6347

Jian Qin − *Department of Chemical Engineering, Stanford University, Stanford, California 94305, United States;* orcid.org/0000-0001-6271-068X

Complete contact information is available at: https://pubs.acs.org/10.1021/jacs.9b11056

Notes

The authors declare no competing financial interest.

ACKNOWLEDGMENTS

C.V.A. is supported by the TomKat Center Postdoctoral Fellowship in Sustainable Energy at Stanford University and the California Alliance Postdoctoral Fellowship. We thank Jianyu Li and Arumugam Manthiram for providing the NMC 811 samples. NMR was performed at the NMR Facility in the Stanford Department of Chemistry. The authors thank Stephen Lynch for help with the NMR experiments. We acknowledge the support from the Assistant Secretary for Energy Efficiency and Renewable Energy, Office of Vehicle Technologies, of the U.S. Department of Energy under the Battery Materials Research (BMR) program and the Battery 500 Consortium program.

REFERENCES

(1) Bruce, P. G.; Freunberger, S. A.; Hardwick, L. J.; Tarascon, J.-M. Li−O2 and Li−S Batteries with High Energy Storage. *Nat. Mater.* **2012**, *11*, 19−29.

(2) Lin, D.; Liu, Y.; Cui, Y. Reviving the Lithium Metal Anode for High-Energy Batteries. *Nat. Nanotechnol.* **2017**, *12*, 194.

(3) Amanchukwu, C. V.; Chang, H.-H.; Gauthier, M.; Feng, S.; Batcho, T. P.; Hammond, P. T. One-Electron Mechanism in a Gel−Polymer Electrolyte Li−O 2 Battery. *Chem. Mater.* **2016**, *28* (19), 7167−7177.

(4) Amanchukwu, C. V.; Chang, H.-H.; Hammond, P. T. Influence of Ammonium Salts on Discharge and Charge of Li−O 2 Batteries. *J. Phys. Chem. C* **2017**, *121* (33), 17671−17681.

(5) Girishkumar, G.; Mccloskey, B.; Luntz, A. C.; Swanson, S.; Wilcke, W. Lithium-Air Battery: Promise and Challenges. *J. Phys. Chem. Lett.* **2010**, *1*, 2193−2203.

(6) Manthiram, A.; Fu, Y.; Su, Y. S. Challenges and Prospects of Lithium-Sulfur Batteries. *Acc. Chem. Res.* **2013**, *46* (5), 1125−1134.

(7) Tikekar, M. D.; Choudhury, S.; Tu, Z.; Archer, L. A.Design Principles for Electrolytes and Interfaces for Stable Lithium-Metal Batteries. *Nat. Energy* **2016**, *1* (9), 16114.

(8) Winter, M.; Barnett, B.; Xu, K. Before Li Ion Batteries. *Chem. Rev.* **2018**, *118* (23), 11433−11456.

(9) Xu, K. Nonaqueous Liquid Electrolytes for Lithium-Based Rechargeable Batteries. *Chem. Rev.* **2004**, *104* (10), 4303−4418.

(10) Jung, R.; Metzger, M.; Maglia, F.; Stinner, C.; Gasteiger, H. A. Oxygen Release and Its Effect on the Cycling Stability of LiNi x Mn y Co z O 2 (NMC) Cathode Materials for Li-Ion Batteries. *J. Electrochem. Soc.* **2017**, *164* (7), 1361−1377.

(11) Etacheri, V.; Marom, R.; Elazari, R.; Salitra, G.; Aurbach, D. Challenges in the Development of Advanced Li-Ion Batteries: A Review. *Energy Environ. Sci.* **2011**, *4*, 3243−3262.

(12) Ding, F.; Xu, W.; Chen, X.; Zhang, J.; Engelhard, M. H.; Zhang, Y.; Johnson, B. R.; Crum, J. V.; Blake, T. A.; Liu, X.; et al. Effects of Carbonate Solvents and Lithium Salts on Morphology and Coulombic Efficiency of Lithium Electrode. *J. Electrochem. Soc.* **2013**, *160* (10), A1894−A1901.

(13) Pei, A.; Zheng, G.; Shi, F.; Li, Y.; Cui, Y. Nanoscale Nucleation and Growth of Electrodeposited Lithium Metal. *Nano Lett.* **2017**, *17*, 1132−1139.

(14) Jiao, S.; Ren, X.; Cao, R.; Engelhard, M. H.; Liu, Y.; Hu, D.; Mei, D.; Zheng, J.; Zhao, W.; Li, Q.; et al. Stable Cycling of High-Voltage Lithium Metal Batteries in Ether Electrolytes. *Nat. Energy* **2018**, *3*, 739−746.

(15) Yoshida, K.; Nakamura, M.; Kazue, Y.; Tachikawa, N.; Tsuzuki, S.; Seki, S.; Dokko, K.; Watanabe, M. Oxidative-Stability Enhancement and Charge Transport Mechanism in GlymeÀLithium Salt Equimolar Complexes. *J. Am. Chem. Soc.* **2011**, *133*, 13121−13129.

(16) Yoshida, K.; Nakamura, M.; Kazue, Y.; Dokko, K.; Watanabe, M. Characterization of Glyme-Lthium Salt Complexes as Ionic Liquids with Li+ Ion Conductivity. *Meeting Abstracts. No. 49. The Electrochemical Society* **2008**, 3022−3022.

(17) Suo, L.; Borodin, O.; Gao, T.; Olguin, M.; Ho, J.; Fan, X.; Luo, C.; Wang, C.; Xu, K. "Water-in-Salt" Electrolyte Enables High-Voltage Aqueous Lithium-Ion Chemistries. *Science* **2015**, *350* (6263), 938−943.

(18) Suo, L.; Hu, Y.-S.; Li, H.; Armand, M.; Chen, L. A New Class of Solvent-in-Salt Electrolyte for High-Energy Rechargeable Metallic Lithium Batteries. *Nat. Commun.* **2013**, *4* (1), 1481.

(19) Lee, C.-W.; Pang, Q.; Ha, S.; Cheng, L.; Han, S.-D.; Zavadil, K. R.; Gallagher, K. G.; Nazar, L. F.; Balasubramanian, M. Directing the Lithium−Sulfur Reaction Pathway via Sparingly Solvating Electrolytes for High Energy Density Batteries. *ACS Cent. Sci.* **2017**, *3* (6), 605−613.

(20) Ueno, K.; Murai, J.; Moon, H.; Dokko, K.; Watanabe, M. A Design Approach to Lithium-Ion Battery Electrolyte Based on Diluted Solvate Ionic Liquids. *J. Electrochem. Soc.* **2017**, *164* (1), A6088−A6094.

(21) Yamada, Y.; Wang, J.; Ko, S.; Watanabe, E.; Yamada, A. Advances and Issues in Developing Salt-Concentrated Battery Electrolytes. *Nat. Energy* **2019**, *4*, 269−280.

(22) See, K. A.; Wu, H.-L.; Lau, K. C.; Shin, M.; Cheng, L.; Balasubramanian, M.; Gallagher, K. G.; Curtiss, L. A.; Gewirth, A. A. Effect of Hydrofluoroether Cosolvent Addition on Li Solvation in Acetonitrile-Based Solvate Electrolytes and Its Influence on S Reduction in a Li−S Battery. *ACS Appl. Mater. Interfaces* **2016**, *8* (50), 34360−34371.

(23) Chen, S.; Zheng, J.; Mei, D.; Han, K. S.; Engelhard, M. H.; Zhao, W.; Xu, W.; Liu, J.; Zhang, J.-G. High-Voltage Lithium-Metal Batteries Enabled by Localized High-Concentration Electrolytes. *Adv. Mater.* **2018**, *30* (21), 1706102.

(24) Borodin, O. Challenges with Prediction of Battery Electrolyte Electrochemical Stability Window and Guiding the Electrode − Electrolyte Stabilization. *Curr. Opin. Electrochem.* **2019**, *13*, 86−93.

(25) Fan, X.; Chen, L.; Borodin, O.; Ji, X.; Chen, J.; Hou, S.; Deng, T.; Zheng, J.; Yang, C.; Liou, S.-C.; et al. Non-Flammable Electrolyte Enables Li-Metal Batteries with Aggressive Cathode Chemistries. *Nat. Nanotechnol.* **2018**, *13* (8), 715−722.

(26) Shah, D. B.; Olson, K. R.; Karny, A.; Mecham, S. J.; DeSimone, J. M.; Balsara, N. P. Effect of Anion Size on Conductivity and Transference Number of Perfluoroether Electrolytes with Lithium Salts. *J. Electrochem. Soc.* **2017**, *164* (14), A3511−A3517.

(27) Olson, K. R.; Wong, D. H. C.; Chintapalli, M.; Timachova, K.; Janusziewicz, R.; Daniel, W. F. M.; Mecham, S.; Sheiko, S.; Balsara, N. P.; DeSimone, J. M. Liquid Perfluoropolyether Electrolytes with Enhanced Ionic Conductivity for Lithium Battery Applications. *Polymer* **2016**, *100*, 126−133.

(28) Chintapalli, M.; Timachova, K.; Olson, K. R.; Mecham, S. J.; Devaux, D.; DeSimone, J. M.; Balsara, N. P. Relationship between Conductivity, Ion Diffusion, and Transference Number in Perfluoropolyether Electrolytes. *Macromolecules* **2016**, *49* (9), 3508−3515.

(29) Wong, D. H. C.; Thelen, J. L.; Fu, Y.; Devaux, D.; Pandya, A. A.; Battaglia, V. S.; Balsara, N. P.; DeSimone, J. M. Nonflammable Perfluoropolyether-Based Electrolytes for Lithium Batteries. *Proc. Natl. Acad. Sci. U. S. A.* **2014**, *111* (9), 3327−3331.

(30) Timachova, K.; Chintapalli, M.; Olson, K. R.; Mecham, S. J.; DeSimone, J. M.; Balsara, N. P. Mechanism of Ion Transport in Perfluoropolyether Electrolytes with a Lithium Salt. *Soft Matter* **2017**, *13* (32), 5389−5396.

(31) Wong, D. H. C.; Vitale, A.; Devaux, D.; Taylor, A.; Pandya, A. A.; Hallinan, D. T.; Thelen, J. L.; Mecham, S. J.; Lux, S. F.; Lapides, A. M.; et al. Phase Behavior and Electrochemical Characterization of Blends of Perfluoropolyether, Poly(Ethylene Glycol), and a Lithium Salt. *Chem. Mater.* **2015**, *27* (2), 597−603.

(32) Tamura, T.; Yoshida, K.; Hachida, T.; Tsuchiya, M.; Nakamura, M.; Kazue, Y.; Tachikawa, N.; Dokko, K.; Watanabe, M. Physicochemical Properties of GlymeLi Salt Complexes as a New Family of Room-Temperature Ionic Liquids. *Chem. Lett.* **2010**, *39* (7), 753−755.

(33) Watanabe, M.; Dokko, K.; Ueno, K.; Thomas, M. L.; Leitner, W.; Kozinski, J. A.; Butler, P. I.; Japan, R.; Ryung Byon, H. Account/Review for Materials Innovation From Ionic Liquids to Solvate Ionic Liquids: Challenges and Opportunities for Next Generation Battery Electrolytes. *Bull. Chem. Soc. Jpn.* **2018**, *91*, 1660−1682.

(34) Wnek, G. E. Structure−Property Relationships of Small Organic Molecules as a Prelude to the Teaching of Polymer Science. *J. Chem. Educ.* **2017**, *94*, 1647−1654.

(35) Salanne, M. Simulations of Room Temperature Ionic Liquids: From Polarizable to Coarse-Grained Force Fields. *Phys. Chem. Chem. Phys.* **2015**, *17*, 14270−14279.

(36) Rajput, N. N.; Murugesan, V.; Shin, Y.; Han, K. S.; Lau, C.; Chen, J.; Liu, J.; Curtiss, L. A.; Mueller, K. T.; et al. Elucidating the Solvation Structure and Dynamics of Lithium Polysulfides Resulting from Competitive Salt and Solvent Interactions. *Chem. Mater.* **2017**, *29*, 3375−3379.

(37) Gunther, H. Lithium NMR. In *Encyclopedia of Magnetic Resonance*; John Wiley & Sons, Ltd: Chichester, UK, 2007. DOI: 10.1002/9780470034590.emrstm0273.

(38) Lukatskaya, M. R.; Feldblyum, J. I.; Mackanic, D. G.; Lissel, F.; Michels, D. L.; Cui, Y.; Bao, Z. Concentrated Mixed Cation Acetate "Water-in-Salt" Solutions as Green and Low-Cost High Voltage Electrolytes for Aqueous Batteries. *Energy Environ. Sci.* **2018**, *11* (10), 2876−2883.

(39) Qiao, B.; Leverick, G. M.; Zhao, W.; Flood, A. H.; Johnson, J. A.; Shao-Horn, Y. Supramolecular Regulation of Anions Enhances Conductivity and Transference Number of Lithium in Liquid Electrolytes. *J. Am. Chem. Soc.* **2018**, *140* (35), 10932−10936.

(40) Amanchukwu, C. V.; Kong, X.; Qin, J.; Cui, Y.; Bao, Z. Nonpolar Alkanes Modify Lithium-Ion Solvation for Improved Lithium Deposition and Stripping. *Adv. Energy Mater.* **2019**, *9* (41), 1902116.

(41) Bloembergen, N.; Purcell, E. M.; Pound, R. V. Relaxation Effects in Nuclear Magnetic Resonance Absorption. *Phys. Rev.* **1948**, *73* (7), 679−712.

(42) Amanchukwu, C. V.; Harding, J. R.; Shao-Horn, Y.; Hammond, P. T. Understanding the Chemical Stability of Polymers for Lithium−Air Batteries. *Chem. Mater.* **2015**, *27* (2), 550−561.

(43) Aspern, N.; Röschenthaler, G.-V.; Winter, M.; Cekic-Laskovic, I. Fluorine and Lithium: Ideal Partners for High-Performance Rechargeable Battery Electrolytes. *Angew. Chem., Int. Ed.* **2019**, *58* (45), 15978−16000.

(44) Horowitz, Y.; Han, H.-L.; Ralston, W. T.; de Araujo, J. R.; Kreidler, E.; Brooks, C.; Somorjai, G. A. Fluorinated End-Groups in Electrolytes Induce Ordered Electrolyte/Anode Interface Even at Open-Circuit Potential as Revealed by Sum Frequency Generation Vibrational Spectroscopy. *Adv. Energy Mater.* **2017**, *7* (17), 1602060.

(45) Huang, M.; Feng, S.; Zhang, W.; Giordano, L.; Chen, M.; Amanchukwu, C. V.; Anandakathir, R.; Shao-Horn, Y.; Johnson, J. A. Fluorinated Aryl Sulfonimide Tagged (FAST) Salts: Modular Synthesis and Structure−Property Relationships for Battery Applications. *Energy Environ. Sci.* **2018**, *11* (5), 1326−1334.

(46) Terada, S.; Mandai, T.; Suzuki, S.; Tsuzuki, S.; Watanabe, K.; Kamei, Y.; Ueno, K.; Dokko, K.; Watanabe, M. Thermal and Electrochemical Stability of Tetraglyme−Magnesium Bis(Trifluoromethanesulfonyl)Amide Complex: Electric Field Effect of Divalent Cation on Solvate Stability. *J. Phys. Chem. C* **2016**, *120*, 1353−1365.

(47) Krause, L. J.; Lamanna, W.; Summerfield, J.; Engle, M.; Korba, G.; Loch, R.; Atanasoski, R. Corrosion of Aluminum at High Voltages in Non-Aqueous Electrolytes Containing Perfluoroalkylsulfonyl Imides; New Lithium Salts for Lithium-Ion Cells. *J. Power Sources* **1997**, *68*, 320−325.

(48) Choudhury, S.; Tu, Z.; Nijamudheen, A.; Zachman, M. J.; Stalin, S.; Deng, Y.; Zhao, Q.; Vu, D.; Kourkoutis, L. F.; Mendoza-Cortes, J. L.; et al. Stabilizing Polymer Electrolytes in High-Voltage Lithium Batteries. *Nat. Commun.* **2019**, *10* (1), 3091.

(49) Swan, I.; Reid, M.; Howe, P. W. A.; Connell, M. A.; Nilsson, M.; Moore, M. A.; Morris, G. A. Sample Convection in Liquid-State NMR: Why It Is Always with Us, and What We Can Do about It. *J. Magn. Reson.* **2015**, *252*, 120−129.

(50) Jorgensen, W. L.; Maxwell, D. S.; Tirado-Rives, J. Development and Testing of the OPLS All-Atom Force Field on Conformational Energetics and Properties of Organic Liquids. *J. Am. Chem. Soc.* **1996**, *118* (45), 11225−11236.

(51) Sambasivarao, S. V.; Acevedo, O. Development of OPLS-AA Force Field Parameters for 68 Unique Ionic Liquids. *J. Chem. Theory Comput.* **2009**, *5* (4), 1038−1050.

(52) Abraham, M. J.; Murtola, T.; Schulz, R.; Páll, S.; Smith, J. C.; Hess, B.; Lindahl, E. GROMACS: High Performance Molecular Simulations through Multi-Level Parallelism from Laptops to Supercomputers. *SoftwareX* **2015**, *1−2*, 19−25.